fact determines the forbidden bandwidth, decreases in its turn with atomic number.

This approach may be useful in trying to explain atomic displacements that bring about ferroelectric, antiferroelectric or ferroelastic properties of heavy-metal compounds.

References

ABRAHAMS, S. C., JAMIESON, P. S. & BERNSTEIN, J. L. (1967). *J. Chem. Phys.* **47**, 4034-4041.

AURIVILLIUS, B. & MALMROS, G. (1972). *K. Tek. Hoegsk. Handl.* **291**, 544-562.

BERSUKER, I. B. (1966). *Phys. Lett.* **20**, 589-590.

CHANUSSOT, G. (1974). *Ferroelectrics*, **8**, 671-683.

FOMCHENKOV, L. P., MAYER, A. A. & GRACHEVA, N. A. (1974). *Izv. Akad. Nauk SSSR*, **10**, 2020-2023 (in Russian).

GATTOW, G. & SCHRÖDER, H. (1962). *Z. Anorg. Allg. Chem.* **318**, 176-189.

HARWIG, H. A. (1978). *Z. Anorg. Allg. Chem.* **444**, 151-166.

KHACHATURYAN, A. G. (1962). *Phys. Met. Metallogr. (USSR)*, **13**, 493-501.

KHACHATURYAN, A. G. (1963). *Sov. Phys. Solid State*, **5**, 16-24, 548-555.

KHACHATURYAN, A. G. (1973). *Phys. Status Solidi B*, **60**, 9-37.

KHACHATURYAN, A. G. (1978). *Prog. Mater. Sci.* **22**, 1-150.

KHACHATURYAN, A. G. & POKROVSKII, B. I. (1985). *Prog. Mater. Sci.* **29**, 1-138.

KRISTOFEL, N. & KONSIN, P. (1967). *Phys. Status Solidi*, **21**, K39-K43.

KRISTOFEL, N. & KONSIN, P. (1968). *Phys. Status Solidi*, **28**, 731-739.

KRISTOFEL, N. & KONSIN, P. (1973). *Ferroelectrics*, **6**, 3-12.

OPIK, U. & PRYCE, M. H. L. (1957). *Proc. R. Soc. London Ser. A*, **238**, 425-447.

ORGEL, L. E. (1959). *J. Chem. Soc.* **12**, 3815-3819.

SILLEN, L. G. (1937). *Ark. Kemi Mineral. Geol.* **12A**, 1-15.

TAKAHASHI, T., ESAKA, T. & IWAHARA, H. (1975). *J. Appl. Electrochem.* **5**, 197-202.

TAKAHASHI, T., ESAKA, T. & IWAHARA, H. (1976). *J. Solid State Chem.* **16**, 317-323.

TAKAHASHI, T., ESAKA, T. & IWAHARA, H. (1977). *J. Appl. Electrochem.* **7**, 31-35.

TAKAHASHI, T. & IWAHARA, H. (1973). *J. Appl. Electrochem.* **3**, 65-72.

TAKAHASHI, T., IWAHARA, H. & ARAO, T. (1975). *J. Appl. Electrochem.* **5**, 187-195.

TAKAHASHI, T., IWAHARA, H. & NAGAI, Y. (1972). *J. Appl. Electrochem.* **2**, 97-104.

VEKHTER, B. G. & BERSUKER, I. B. (1973). *Ferroelectrics*, **6**, 13-14.

WILLIS, B. T. M. (1963). *Proc. R. Soc. London Ser. A*, **274**, 134-144.

WILLIS, B. T. M. (1964). *J. Phys. Radium*, **25**, 431-439.

WILLIS, B. T. M. (1965). *Acta Cryst.* **18**, 75-76.

ZAVYALOVA, A. A. & IMAMOV, R. M. (1969). *Sov. Phys. Crystallogr.* **14**, 331-334.

ZAVYALOVA, A. A. & IMAMOV, R. M. (1971). *Sov. Phys. Crystallogr.* **16**, 516-519.

Acta Cryst. (1986). B**42**, 224-229

Electron-Beam Damage Observed in the Fast Proton Conductor Ammonium/Hydronium β''-Alumina:* a High-Resolution Electron Microscope (HREM) Study†

BY A. K. PETFORD

Center for Solid State Science, Arizona State University, Tempe, Arizona 85287, *USA*

AND C. J. HUMPHREYS

Department of Metallurgy, University of Liverpool, PO Box 147, *Liverpool, England*

(*Received* 28 *March* 1985; *accepted* 5 *November* 1985)

Abstract

Crystals of ceramic ammonium/hydronium β''-alumina [formula $(NH_4)_{1\cdot67-y}(H_3O)_yMg_{0\cdot67}AL_{10\cdot33}O_{17}\cdot(H_2O)_x$] have been examined in a JEOL 200CX high-resolution electron microscope and high-resolution images obtained of the electron-beam-induced damage. The material is of interest owing to its potential use as a fast proton conductor. Two of the damage modes reported have not previously been seen in the β''-aluminas – secondary proton damage and the formation of small gas bubbles within the material. Mechanisms for these two damage modes are proposed. The other damage mode (loss of the cation-containing planes) is the most common result of electron-beam damage in these materials and the collapse vectors present in ammonium/hydronium β''-alumina are discussed.

The structure of the β-aluminas

The β-aluminas are a family of polyaluminates of which the first to be characterized was sodium β-alumina (Bragg, Gottfried & West, 1931) of formula $Na_2O.11Al_2O_3$. Binary sodium β''-alumina (formula $Na_2O.5Al_2O_3$) was first reported by Théry & Briançon (1962). The hexagonal cell of β-alumina contains two 11 Å thick spinel-like layers, of close-packed aluminium and oxygen atoms, which lie perpendicular to the c axis. The spinel blocks are separated

* IUPAC name: ammonium/oxonium β''-alumina.

† Work carried out in the Department of Metallurgy and Science of Materials, Parks Road, Oxford OX1 3PH, England.

0108-7681/86/030224-06$01.50

by loosely packed layers containing oxygen and sodium and are held apart by Al–O–Al bridges. The blocks are related by a mirror plane in the sodium-containing layer (known as the conduction plane). The atomic spacing is such as to allow two-dimensional motion of the alkali ions within the conduction planes leading to high ionic conductivity.

The hexagonal cell usually considered for β''-alumina has $c = 3/2\times$ that of β-alumina, and contains three spinel blocks related by a threefold screw axis parallel to c. The hexagonal cell of β''-alumina contains three of the primitive rhombohedral unit cells (space group $R\bar{3}m$). The unit cell of β or β''-alumina contains a large number of oxygen atoms. In order to distinguish between them, each distinct crystallographic site is identified by a number. For example, the bridging oxygen site is known as the O(5) site.

Binary β''-alumina is only stable in dry conditions and is usually stabilized by the addition of MgO or Li_2O to give a ternary compound such as $Na_2O.MgO.5Al_2O_3$ (Bettman & Peters, 1969).

β and β''-aluminas containing cations other than sodium have been prepared, usually by direct ion exchange in the appropriate molten salt (Yao & Kummer, 1967). One such material is ammonium/hydronium β''-alumina [formula $(NH_4)_{1\cdot67-y}(H_3O)_yMg_{0\cdot67}Al_{10\cdot33}O_{17}.(H_2O)_x$] (Thomas & Farrington, 1983) which has lattice parameters $a = 5\cdot631$, $c = 34\cdot378$ Å.

The high conductivity of ammonium/hydronium β''-alumina is due to the following: each NH_4^+ vacancy in the conduction planes is occupied by either an H_2O molecule or an H_3O^+ ion. The H_xO groups form a two-dimensional Grotthus-type network through the conduction planes (Thomas & Farrington, 1983): protons are transported by hopping from the H_3O^+ ions to the H_2O molecules.

Some motion of the NH_4^+ cations has been observed (Ochadlick, Bailey, Stamp, Story, Farrington & Briant, 1979) using NMR techniques, but it seems likely that the conductivity of the ammonium/hydronium β''-alumina is predominantly due to the Grotthus H^+ motion (Thomas & Farrington, 1983). The ionic conductivity of the material is $10^{-3}\,\Omega^{-1}\,m^{-1}$ at 298 K, rising to $10^{-2}\,\Omega^{-1}\,m^{-1}$ at 473 K (Thomas & Farrington, 1983), which is considerably higher than that of other solid proton conductors such as $HUO_2PO_4.4H_2O$, with a conductivity of $\sim 10^{-4}\,\Omega^{-1}\,m^{-1}$ at 298 K (Shilton & Howe, 1977).

NH_4^+/H_3O^+ β''-alumina is the only known solid proton conductor to maintain its composition and conductivity to at least 498 K – an important consideration, since fuel cells containing solid proton-conducting electrolytes are expected to operate at temperatures of around 473 K. [For references to the use of solid proton conductors in fuel cells see, for example, Thomas & Farrington (1983), Shilton & Howe (1977) and McGeehin & Hooper (1977).]

Conduction-plane loss in the β''-aluminas

Exposure to an electron beam results in the loss of mobile cations and bridging oxygens from the conduction planes with a subsequent collapse of the material to form broad spinel blocks. This has been observed by high-resolution electron microscopy (HREM) in sodium and various other β''-aluminas by many workers. Models have been proposed (De Jonghe, 1977; Bovin, 1979; Matsui & Horiuchi, 1981) to explain the HREM images obtained before and after collapse.

HREM of defect-free β''-alumina gives rise to images containing rows of large tunnels – the conduction planes (imaged as large white dots) – separating regions each containing one row of small tunnels – the spinel blocks. When a conduction plane collapses the defect formed is imaged as two rows of large white dots enclosing three rows of smaller white dots – representing two conduction planes on either side of a broad spinel block.

Fig. 1(*a*) illustrates the two distinct images obtained of such defect blocks: in defect type *A*, the tunnels in the defect block are aligned at approximately 20° to the *c* axis, and the tunnels in the conduction planes on either side are aligned parallel to the *c* axis. In defect type *B*, the outermost rows of tunnels in the defect spinel block are aligned parallel to **c**, whilst the central row appears indistinct. The conduction-plane tunnels are mutually displaced normal to **c** with each tunnel in the upper conduction plane lying approximately midway between two tunnels in the lower one. The conduction-plane tunnel arrangement on either side of the defect block for type *A* and *B* defects is shown in Fig. 1(*b*).

Matsui & Horiuchi (1981) observed both types of defect in sodium β''-alumina and determined the slide vectors involved. They arrived at three slide vectors, $\mathbf{V}_i$, composed of a collapse in the **c** direction plus a shear vector:

$$\mathbf{V}_1 = a/6 + b/3 + \mathbf{V}_c$$
$$\mathbf{V}_2 = -a/3 - b/6 + \mathbf{V}_c$$
$$\mathbf{V}_3 = a/6 - b/6 + \mathbf{V}_c.$$

($\mathbf{V}_c$ = collapse in **c** direction; a, b are the lattice parameters of β''-alumina.)

The three slide vectors are related by a 120° rotation around the *c* axis and in β''-alumina are crystallographically equivalent. Thus, the defect blocks are structurally the same except for their orientation with respect to the host lattice.

Matsui & Horiuchi could explain the two types of defect imaged by this model, by comparison of the

experimental HREM images with computer-calculated images. In images taken with the electron beam parallel to the [11$\bar{2}$0] direction, $\mathbf{V}_1$ gives rise to defect type *A* and $\mathbf{V}_2$ and $\mathbf{V}_3$ to defect type *B*.

The shear vectors proposed correspond to the bridging AlO_4 tetrahedra losing the corner-shared bridging oxygen and sliding together to become edge sharing.

Heat treatment can also lead to conduction-plane loss, owing to the need to preserve stoichiometry when ammonium ions are lost from the conduction planes. Care must be taken to distinguish between planes lost due to electron-beam exposure, and those already missing from the crystal. If the beam is initially spread (giving a low current density at the sample), so that no beam damage occurs, the original defect density can be measured. If the beam is then focused down an estimate can be made of the rate of conduction-plane loss due to beam damage.

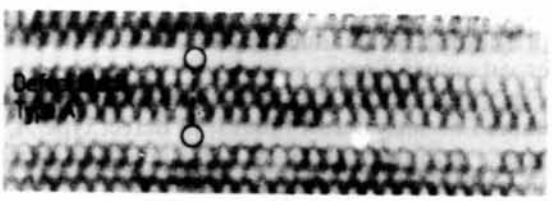

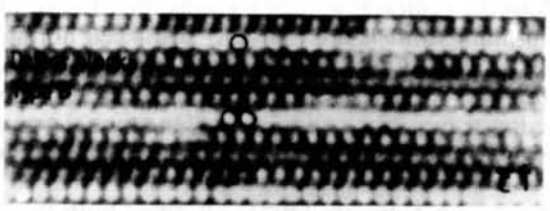

(*a*)

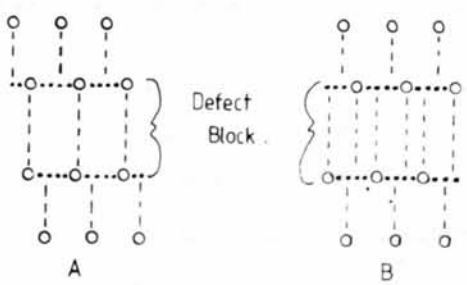

(*b*)

Fig. 1. (*a*) HREM images of irradiation-induced defects showing *A*- and *B*-type defects. See text for further explanation of this figure. (*b*) Schematic representation of the arrangement of tunnels (open circles) on either side of the irradiation-induced defect blocks expected from the Matsui & Horiuchi model. [The vertical scale in (*b*) is artificially reduced.]

Experimental procedure

The material was prepared by ion exchange of magnesium-stabilized sodium β''-alumina in ammonium nitrate (Thomas & Farrington, 1983). Its composition, as determined by neutron diffraction, was $(NH_4^+)_{1\cdot56}(H_3O^+)_{0\cdot19}Mg_{0\cdot75}Al_{10\cdot25}O_{17}.(H_2O)_{0\cdot25}$. The sample was first heated to 720 K and cooled again, during which time ammonia was given off, leaving a 42% ammonium ion content in the β''-alumina.

The crystalline sample was prepared for electron microscopy by crushing under a mixture of chloroform and liquid nitrogen to produce a fine powder. A small amount of the powder was deposited on a holey-carbon-film-coated copper grid, for examination in the JEOL 200CX HREM at Oxford. In order to minimize electron-beam damage upon initial electron irradiation, the electron beam was spread to give the minimum illumination necessary for observing at a direct magnification of about 3×10^5.

The JEOL 200CX at Oxford has a top-entry dual-tilt specimen holder with tilt ±10°, allowing the crystallites to be aligned in the desired orientation.

In this particular study, images were obtained with the electron beam parallel to the [11$\bar{2}$0] zone axis. In this orientation the bridging oxygens are aligned in columns parallel to the beam direction with tunnels containing the cation positions between the columns of bridging oxygens in the O(5) sites (see Fig. 2).

HREM observations

Fig. 3 shows a region of the ammonium/oxonium β''-alumina after exposure to the electron beam for

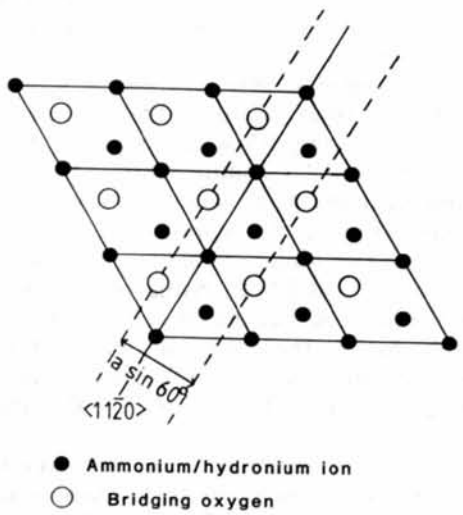

Fig. 2. Schematic diagram showing the relationship between the ⟨1120⟩ direction and the conduction-plane structure in ammonium/hydronium β''-alumina. The positions of the ammonium/hydronium ions and the bridging oxygens, occupying the crystallographic O(5) sites, are shown.

~20 min. Many of the conduction planes have been lost, leaving broad defect spinel blocks. The most dominant spacing visible corresponds to defect blocks with a thickness of 20·6 Å – formed when a single conduction plane is lost. A partially collapsed conduction plane is indicated with dashed arrows. Defects of type *A* and *B* as described above and in Fig. 1 are indicated. Also visible are small light patches (circled) which increase in number as electron-beam irradiation continues; a damage mode not previously seen in HREM studies of the β''-aluminas.

The final damage observed in the ammonium/hydronium β''-alumina is illustrated in Fig. 4: a defect on the left-hand side of the image in (*a*) has grown during exposure, and a second similar defect has formed. The three exposures were taken at intervals of approximately 30 s. As far as we know, this damage mode has also not previously been reported in the β''-aluminas.

Discussion

Analysis of the broad defect blocks, formed as a result of conduction-plane loss, shows that the collapse vectors for ammonium/hydronium β''-alumina (leading to the formation of a broad defect block) are the same as those proposed by Matsui & Horiuchi for sodium β''-alumina.

The method used to calculate the slide and collapse vectors was that used by Matsui & Horiuchi (1981) and involved a comparison between the relative displacement of the conduction-plane tunnels on either side of spinel blocks in

(i) a defect-free region of the material, and

(ii) those on either side of a broad defect block.

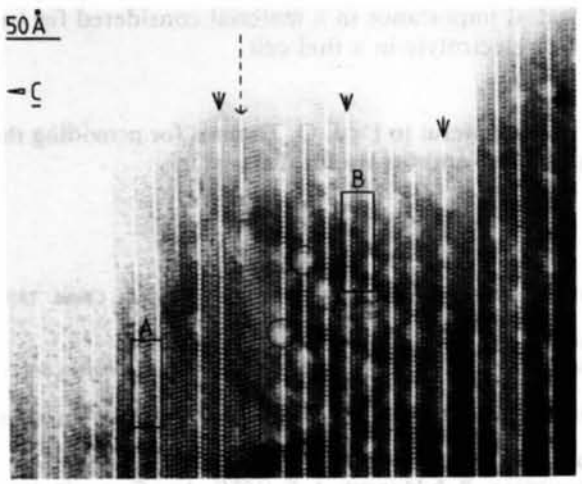

Fig. 3. Lattice image of ammonium/hydronium β''-alumina showing defects due to knock-on damage caused by protons in the conduction planes; examples of defects are circled. Defects of type *A* and type *B* due to the loss of conduction planes are indicated. See text for further explanation of defects. The positions of some of the conduction planes are marked with arrows.

The broad spinel block labelled *A* in Fig. 3 corresponds to that formed by the action of slide vector $\mathbf{V}_1$, and type *B* corresponds to that formed by the action of $\mathbf{V}_2$ or $\mathbf{V}_3$ (see above for explanation of the slide vector rotation).

The pale patches circled in Fig. 3 correspond to regions of decreased density or thickness in the specimen. A comparison was made between computed images [calculated using the multislice technique (Goodman & Moodie, 1974)] and the experimental images. This shows that at the microscope defocus used, regions of high atomic density – such as the spinel blocks – will appear dark, and regions of low atomic density will appear light. This leads us to propose that the pale regions formed during exposure to the electron beam are due to a local decrease in atomic density. These defects are thought to be due

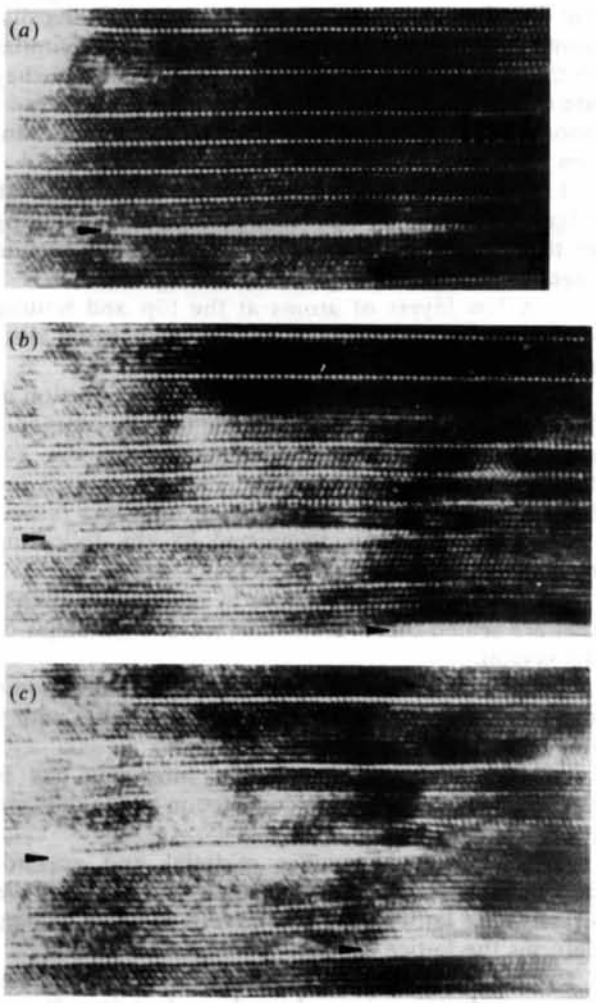

Fig. 4. HREM image of ammonium/hydronium β''-alumina showing formation and growth of NH_3 bubbles under the electron beam. The images shown in (*a*), (*b*) and (*c*) were taken at intervals of approximately 30 s. The defects are arrowed. The growth mechanism of the defects is discussed in the text.

to knock-on damage by the protons on the NH_4^+ and H_3O^+ groups in the conduction planes: an incident electron displaces a proton within a conduction plane - these protons are then free to act as an ion beam, causing displacement damage in the surrounding material. This is a very efficient damage mode, as a consideration of conservation of energy and momentum shows that an electron can transfer more energy to an atom *via* a proton than it can if acting alone.

This hypothesis is supported by the fact that damage is always centred on a conduction plane, and by the fact that a similar damage mode has not been observed in other β- or β''-aluminas containing cations heavier than protons. In these cases the cations are too heavy to be displaced by an incident electron and then cause secondary ion damage.

The defects shown in Fig. 4 appear light in an image in which atoms are dark and tunnels are light, suggesting that they are also regions of low atomic density. Some structure is visible within the defects, similar to that in the spinel blocks. It is suggested that they are ammonia bubbles, which increase in size as radiation continues. The proposed defect growth mechanism is as follows:

1. A conduction plane starts to collapse from both edges of the crystal, with loss of ammonia, resulting in the formation of a closed length of conduction plane with broad spinel blocks at either end.

2. A few layers of atoms at the top and bottom surfaces of the crystal collapse so that a sealed 'disc' of conduction plane is left.

3. Further electron irradiation causes reduction of NH_4^+ ions in the conduction plane to form ammonia gas molecules. The pressure exerted by the gas molecules on the walls of the 'bubbles' causes the bubbles to grow, deforming the surrounding lattice.

This mechanism is supported by the following evidence:

(*a*) The defects only occur in conduction planes that are sealed off from the surface at both edges of the crystal.

(*b*) The defects are of low density, but have some structure - this would be true of a gas bubble with a few layers of spinel above and below.

(*c*) As mentioned previously, ammonia gas is known to be evolved when conduction-plane collapse occurs.

(*d*) The defects contain material and are not cracks, as growth of empty cracks occurs to relieve stress in the lattice, whereas growth of these defects deforms the lattice further.

Cracks can appear in β''-alumina in regions where many conduction planes have been lost (*e.g.* Bovin & O'Keeffe, 1980). We have also observed this phenomenon in large crystals. In our observations, crack propagation occurred along existing conduction planes, and was never observed in the smaller crystals (1000-2000 Å) normally examined in the HREM (as in this study). Cracks of this type were only observed in sodium β''-alumina that had been cycled in a sodium/sulfur cell, and were present before exposure to the electron beam. No further cracks were seen to form due to electron-beam irradiation. The defects shown in Fig. 4 only occurred after exposure to the electron beam.

Loss of conduction planes followed by collapse and shear of the surrounding material has been observed in ammonium/hydronium β''-alumina. A model previously proposed for the collapse vectors in sodium β''-alumina has been found to fit the experimental results obtained for collapse in ammonium/oxonium β''-alumina. Two further damage modes, previously unreported in the β''-aluminas, have been observed in this material: the formation of low-density regions centred on the conduction planes, thought to be due to knock-on damage caused by the protons in the conduction plane, and the formation of ammonia bubbles within regions of conduction plane sealed from the surface of the crystal.

The exact structure of the defect spinel blocks is at present unknown, although the HREM images suggest that the blocks consist of layers of γ-alumina separated by stacking faults to preserve stoichiometry.

Although the conditions in the high-vacuum system of the electron microscope are not the same as those of a fuel cell, we feel that information obtained using this technique can still be of use. In both cases ion transport is of importance and, as has been shown, this can cause the growth of defects. The loss of conduction planes is of special interest, as this will lower the ionic conductivity of the ammonium/hydronium β''-alumina - the property of greatest importance in a material considered for use as an electrolyte in a fuel cell.

I am grateful to Dr J. O. Thomas for providing the specimens and for useful discussions.

References

BETTMAN, M. & PETERS, C. R. (1969). *J. Phys. Chem.* **73**(6), 1774-1780.

BOVIN, J.-O. (1979). *Acta Cryst.* A**35**, 572-580.

BOVIN, J.-O. & O'KEEFFE, M. (1980). *Naturwissenschaften*, **66**(11), 576-578.

BRAGG, W. L., GOTTFRIED, C. & WEST, J. (1931). *Z. Kristallogr.* **77**, 255-274.

DE JONGHE, L. C. (1977). *Mater. Res. Bull.* **12**, 667-674.

GOODMAN, P. & MOODIE, A. F. (1974). *Acta Cryst.* A**30**, 280.

MCGEEHIN, P. & HOOPER, A. (1977). *J. Mater. Sci.* **12**, 1-7.

MATSUI, Y. & HORIUCHI, S. (1981). *Acta Cryst.* A**37**, 51-61.

OCHADLICK, A. R., BAILEY, W. C., STAMP, R. L., STORY, H. S., FARRINGTON, G. C. & BRIANT, J. L. (1979). In *Fast Ionic Transport in Solids*, edited by P. D. VASHISHTA, J. N. MUNDY & G. K. SHENOY, p. 401. New York: North-Holland.

SHILTON, M. G. & HOWE, A. T. (1977). *Mater. Res. Bull.* **12**, 701-706.
THÉRY, J. & BRIANÇON, D. (1962). *C. R. Acad. Sci.* **254**, 2782-2784.
THOMAS, J. O. & FARRINGTON, G. C. (1983). *Acta Cryst.* B**39**, 227-235.
YAO, Y. Y. & KUMMER, J. T. (1967). *J. Inorg. Nucl. Chem.* **29**, 2453-2475.

Acta Cryst. (1986). B**42**, 229-236

An Analysis of the Structural Characteristics of Hollandite Compounds

BY ROBERT W. CHEARY

School of Physics and Materials, New South Wales Institute of Technology, PO Box 123, *Broadway, New South Wales, Australia* 2007

(*Received* 29 *April* 1985; *accepted* 18 *November* 1985)

Abstract

Neutron powder diffraction data for seven SYNROC-related barium hollandites $Ba_x(M^{3+}Ti^{4+})_8O_{16}$ have been refined to establish how various trivalent ions such as Fe, Al and Ga change the crystal structure and predispose it to radwaste substitution. Particular attention is given to changes in the environment of the tunnel sites and the nature of the monoclinic-tetragonal transformation in hollandites. Structural data from earlier refinements are included in the analysis. The unit-cell volume, the lattice parameter of the unique axis, the O octahedral volume and the tunnel-cavity volume are all controlled primarily by the size of the octahedral-site cations. The change from tetragonal to monoclinic symmetry occurs when the tunnel cations are no longer able to support the tunnel walls which collapse onto the tunnel ions with the corner linkages between the walls acting as hinges.

Introduction

The synthetic mineral assemblage known as SYNROC is currently being evaluated for the immobilization of radioactive wastes (*e.g.* Kesson & Ringwood, 1984). In this material barium hollandite is used as the host for large cations such as Cs and Rb. The unit-cell formula of hollandites is $A_xB_8O_{16}$ ($x \leq 2$) where A represents ions in the tunnel cavities of the structure (*e.g.* Ba, Cs) and B are smaller cations occupying octahedral sites such as Al^{3+}, Ti^{3+} and Ti^{4+} (Kesson, 1983). They may be tetragonal [$I4/m$, a = 9·90 to 10·10 Å and c = 2·9 to 3·0 Å (Byström & Byström, 1950; Dryden & Wadsley, 1958; Sinclair, McLaughlin & Ringwood, 1980)] or monoclinic [$I2/m$, β = 90 to 91·5° (Cadée & Verschoor, 1978; Post, Von Dreele & Buseck, 1982)]. The symmetry is usually monoclinic when the ratio of the cation radii $R_A/R_B < 2{\cdot}08$ and tetragonal when this ratio $> 2{\cdot}08$ although this is by no means a general rule for all hollandites (Post *et al.*, 1982). In their analysis of radwaste substitution in SYNROC, Kesson (1983) and Kesson & White (1986) have shown that high concentrations of Cs can be immobilized in host hollandites containing Ti^{3+} on the B sites. The majority of hollandites considered in this context are in the solid-solution range between tetragonal $Ba_x(Al^{3+}Ti^{4+})_8O_{16}(x = 1{\cdot}14)$ and monoclinic $Ba(Ti^{3+}Ti^{4+})_8O_{16}$. Presumably, the effect of large ions such as Ti^{3+} on the B sites is to increase the unit-cell volume and enlarge the A-site tunnel cavities thereby facilitating the inclusion of Cs into the structure.

The objective of the present work is to examine how the barium hollandite structure responds to various combinations of M^{3+} and Ti^{4+} ions on the B sites. Particular attention is focused on the following aspects of the structure: the way in which the size and shape of the tunnel sites and the surrounding O octahedral framework change, the factors controlling the monoclinic-tetragonal transformation, and the changes that occur during a structural transformation. Altogether seven barium hollandite structures have been refined, four monoclinic and three tetragonal, from high-resolution neutron powder diffraction data with M = Ga, Al, Fe and varying proportions of Fe and Al. Results from earlier refinements have also been included in this analysis.

Sample preparation and measurement conditions

Initially four barium hollandite specimens were prepared, three tetragonal with M = Al, at two values of x, and Ga (Guha, Kolar & Volavsek, 1976; Cheary, Hunt & Calaizis, 1981; Roth, 1981; Bursill & Grzinic, 1980), and one monoclinic with M = Fe (Cadée & Verschoor, 1978). Three of them were prepared by mixing the starting materials $BaCO_3$, TiO_2 and the appropriate sesquioxide (Al_2O_3, Fe_2O_3 or Ga_2O_3) to give hollandites with x = 1·33 Ba ions per unit cell, *viz.*

$$BaCO_3 + M_2O_3 + 4TiO_2.$$

0108-7681/86/030229-08$01.50